Variability of internal tide energy, mixing and nitrate fluxes in response to changes in stratification on the northeast New Zealand continental shelf

Jonathan Sharples & John R. Zeldis

Published online: 22 Dec 2019.

Submit your article to this journal ↗

Article views: 451

View related articles ↗

View Crossmark data ↗

RESEARCH ARTICLE   👐 OPEN ACCESS   🔄 Check for updates

Variability of internal tide energy, mixing and nitrate fluxes in response to changes in stratification on the northeast New Zealand continental shelf

Jonathan Sharples 🅾 [a] and John R. Zeldis[b]

[a]School of Environmental Sciences, University of Liverpool, Liverpool, UK; [b]National Institute of Water and Atmospheric Research Ltd., Christchurch, New Zealand

ABSTRACT

A 4-month time series of water column temperature structure on the shelf of North Island New Zealand is used to calculate the energy in the internal tide as stratification evolved between spring and summer. Average total energy in the internal tidal wave was 200 J m^{-2}, with peaks reaching 600 J m^{-2}. Wave energy was weakly correlated with stratification ($r = 0.2$) and with the spring-neap cycle of tidal currents ($r = 0.17$). Overall there was little predictability in internal tide behaviour in response to the physical environment. Reduction in wave energy was associated with a downwelling-favourable wind event which reduced stratification by mixing and by removing deeper water off the shelf. Vertical eddy diffusivity driven by internal wave dissipation ranged between 5.6×10^{-5} and 3.2×10^{-4} m^2 s^{-1}. Combined with nitrate data this diffusivity resulted in diapycnal nitrate fluxes towards the sea surface of 1.6–2.2 mmol m^{-2} day^{-1}. Strong stratification in summer reduced the eddy diffusivity but had little effect on nitrate flux as a strengthened vertical nitrate gradient compensated for the reduced diffusivity. This compensation will be important when predicting how stronger stratification in a warmer climate might alter diapycnal nutrient supplies to the upper ocean.

Introduction

Internal tidal waves are a common feature in stratified oceans, caused by the interaction between barotropic tidal currents and sloping seabed (Garrett and Kunze 2007). These waves are found in the open ocean associated with mid-ocean ridges and seamounts (e.g. Noble and Mullineaux 1989; Ledwell et al. 2000; Rudnick et al. 2003; Vic et al. 2018), at the continental shelf edge and slope (e.g. Wunsch and Hendry 1972; New and Pingree 1990), and associated with banks in shelf seas (e.g. Dewey et al. 2005; Palmer et al. 2013). In the open ocean internal tides have become increasingly recognised as important for mixing heat and salt, and maintaining the vertical density structure of the abyssal ocean (Munk and Wunsch 1998; Waterhouse et al. 2014), and more recently for mixing nutrients vertically in the upper ocean (Stevens et al. 2012; Tuerena et al. 2019).

CONTACT Jonathan Sharples ✉ jons@liverpool.ac.uk

Over the continental slopes and in shelf seas the vertical mixing caused by breaking internal tidal waves significantly increases the fluxes of nutrients upwards into the photic zone (e.g. Sharples et al. 2007; Tweddle et al. 2013) and can play a role in structuring plankton communities and supporting commercially-important fisheries (Sharples et al. 2009). In shelf seas the vertical movement of the sub-surface chlorophyll layer by internal tidal waves can provide a pumping mechanism for the food supply to seafloor ecosystems (Witman et al. 1993). Internal tides have also been implicated in the behaviour of schooling fish (Embling et al. 2013). Internal tidal waves are thus of importance on global and regional scales, and are a key physical process underpinning the physical structure of the ocean, biogeochemical fluxes and cycling, and ecosystem structure.

New Zealand's location on the plate boundary between the Pacific and Australian plates, with a number of steep ocean ridges including the Colville and Kermadec ridges to the north and Macquarie Ridges to the south, make the region globally significant in the generation and dissipation of internal tidal waves (e.g. Waterhouse et al. 2014). Direct observations of internal tides have been made around New Zealand, both in the deep ocean over ridges and along the continental slope (Stanton 1977; Vennell and Moore 1993; Chiswell and Moore 1999; Stevens et al. 2005; Waterhouse et al. 2018).

The focus of this paper is on the seasonal-scale variability in the internal tidal wave energy on the northeast shelf of North Island, New Zealand, and the implications for vertical mixing and the diapycnal nitrate supply to surface waters. The northeast shelf has relatively weak barotropic tidal flows (Sharples and Grieg 1998), with maximum tidal current speeds of typically <10 cm s^{-1} and as a result very weak boundary mixing generated by tidal current friction with the seabed. An internal tidal wave is generated over the continental slope, at a depth of around 600–700 m, and propagates over the shelf edge (depth about 130 m) and onto the shelf (Sharples et al. 2001a; Stevens et al. 2005). Satellite imagery (synthetic aperture radar) shows the internal tidal wave on the shelf to have a continuous wavefront, with wavelength about 15 km, followed by packets of smaller wavelength (~1 km) internal waves (Sharples et al. 2001a). These smaller wavelength waves indicate breaking of the main internal tidal wave, and are largely responsible for driving increased vertical mixing with eddy diffusivity of >10^{-4} m^2 s^{-1} (Sharples et al. 2001a; Stevens et al. 2005). This high rate of vertical mixing on the shelf plays an important role in the shelf biogeochemistry. A persistent feature of the northeast shelf is upwelling of cold, nutrient-laden slope water as a result of Ekman transport through the bottom boundary layer of the along-slope East Auckland Current combined with episodic pulses of upwelling-favourable winds (e.g. Zeldis 2004; Zeldis et al. 2004). This upwelling system breaks down in summer, as the shelf is capped by a surface layer of subtropical water, initially driven onto the shelf by downwelling-favourable winds and significantly increasing the shelf stratification (Sharples 1997; Zeldis et al. 2004). Diapycnal mixing of nutrients into the photic zone by the internal tide is likely to be the dominant mechanism of connecting surface shelf waters with the upwelled nutrients through spring and summer, and also supplying new nutrients upward to the oligotrophic surface waters in late summer condition, with much lower contributions from wind-driven mixing (Sharples et al. 2001a).

Analyses of internal tide behaviour and mixing on the northeast shelf have so far been based on short time series of mooring data, typically 10–12 days (Sharples et al. 2001a; Stevens et al. 2005). Here we use a 4-month time series of temperature structure from a

mid-shelf mooring to assess the variability in the internal tide energy and mixing. The time series covers the period from spring through to mid-summer, including the spring-early summer upwelling period and the late summer capping of the shelf with subtropical water. We investigate how wind stress, the spring-neap tidal cycle, and changes in stratification can affect the strength of the internal tide and estimate the consequences for diapycnal mixing of new nutrients upward into the photic zone over the shelf.

Data and methods

Mooring, CTD and wind data

Data were collected by a mooring comprising a series of Hugrun mini temperature loggers and Aanderaa RCM6 current meters on the mid shelf of northeast North Island, New Zealand (Figure 1). In a total water column depth of 100 m, RCM6 current meters
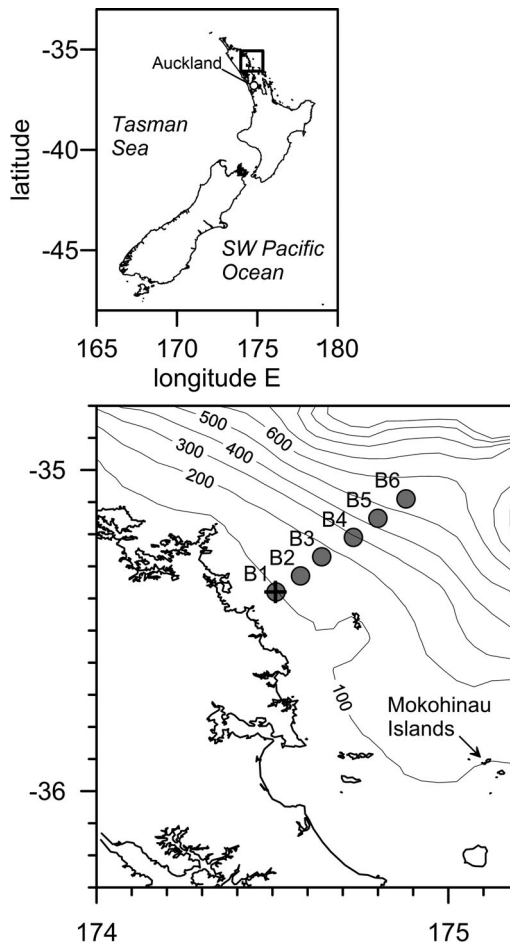

Figure 1. Location of the study area on the northeast shelf of North Island, New Zealand. Bathymetry in the main map is in metres. Filled circles B1–B6 are the locations of the CTD stations, and the cross at B1 is the location of the mooring. Wind velocity data were available from a weather station on the Mokohinau Islands.

(sample period 10 min) were positioned 20 m below the sea surface and 10 m above the seabed. Hugrun loggers (sample period 5 min) were located between the RCMs, at depths of 30, 40, 60 m. Cross-shelf context in the physical structure of the water column was provided by four CTD surveys along a line of stations from the mooring to the continental slope (stations B1–B6 in Figure 1) conducted when the mooring was deployed (September 1996 using a Guildline CTD), serviced (October and December 1996 using a Seabird 911 CTD) and recovered (January 1997, using a Seabird 911 CTD). CTD salinity measurements were calibrated using water samples collected by the CTD rosette and analysed on a Guildline Autosal against standard seawater: the error estimate for salinity was 0.005 (PSS78). Hourly wind speed and direction data were available from an automatic weather station on Mokohinau Island (NIWA National Climate Centre; Figure 1). A full description of the physical environment on the northeast shelf over the period of the mooring deployment can be found in Zeldis et al. (2004).

Analysis for internal tidal wave energy and dissipation

Temperature time series from the moored loggers and RCMs were linearly interpolated onto a regular grid, with 5 m vertical resolution between the sea surface and a nominal depth of 100 m and a time step of 10 min. Temperature values above the upper RCM (depth 20 m) and below the deepest RCM (90 m) were interpolated to the surface and seabed boundaries by extrapolating the vertical temperature gradient; this helps with visual interpretation of the temperature structure, but does not affect the subsequent analyses for the internal wave energy (see below).

Analysis for the potential energy of the internal tidal wave followed an established technique (e.g. Sherwin 1988; Largier 1994; Sharples et al. 2001a). An example of the temperature time series for a single temperature logger on the mooring is shown in Figure 2A,B, illustrating the semi-diurnal variability in temperature superimposed on longer-term low frequency variability. Power spectrum analysis (Figure 2C) shows the importance of the M2 tidal signal in the temperature time series, and that there may be small but potentially significant energy in the M4 harmonic. The energy in the broad shoulder of the spectrum around M4 is perhaps to be expected, knowing that the internal tidal wave does steepen and break (e.g. the SAR imagery in Sharples et al. 2001a).

The water column integrated potential energy, PE (J m^{-2}), of the internal tidal wave in a depth h (metres) is given by

$$PE = \frac{1}{4} \int_{-h}^{0} N(z)^2 \rho(z) \eta_0(z)^2 \mathrm{d}z \tag{1}$$

with $N(z)$ (s^{-1}) the buoyancy frequency and ρ (kg m^{-3}) the density at depth z. The variable $\eta_0(z)$ (metres) is the amplitude of the vertical excursion of the internal tidal wave. At each depth in the interpolated temperature grid the time series was first filtered using a running 12.5 h mean to yield a corresponding grid of the time variation in the mean temperature profile. Then at each time step the excursion of the temperature structure at each grid point was calculated by assessing where on the mean temperature profile at that time the instantaneous value of temperature must have come from. Thus, for each depth on the temperature time series grid a time series of the instantaneous vertical excursion away
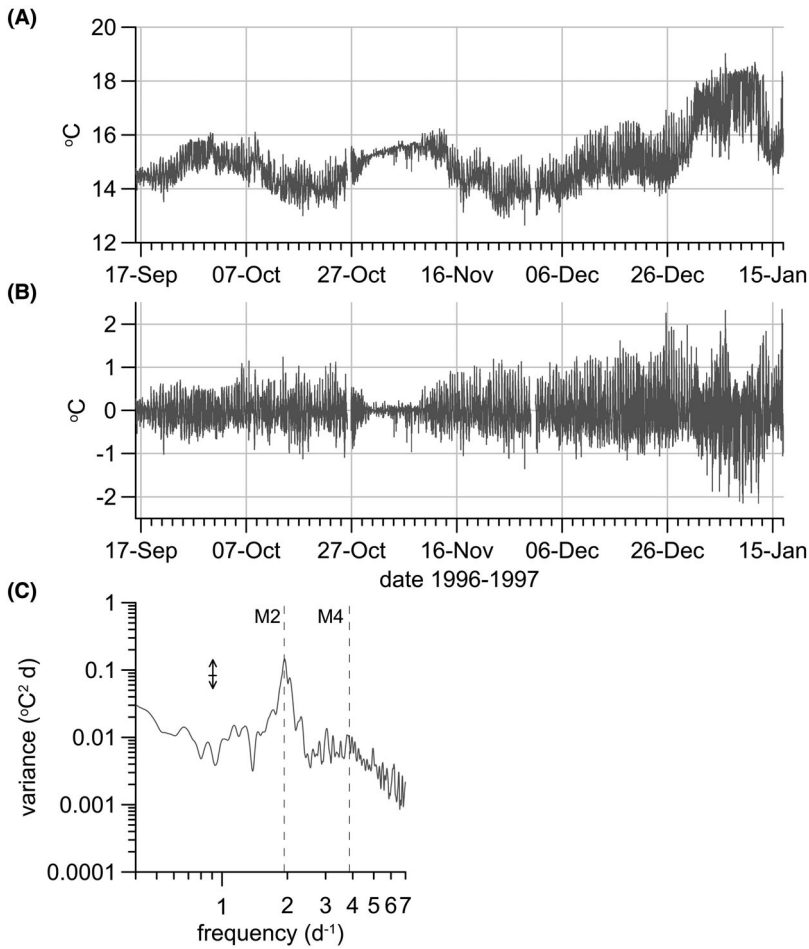
Figure 2. A, Time series from the temperature logger 40 m below the sea surface. **B,** High frequency temperature variability from the data in A, calculated by removing a running 12.5 h mean from the raw time series. **C,** Power spectrum of the temperature signal in A, showing also the periods of the M2 and M4 tidal constituents. The vertical bar indicates the level of 90% uncertainty.

from the mean temperature profile was calculated. The tidal amplitude of the excursion, $\eta_0(z)$, was then calculated at each depth by performing a harmonic analysis of the excursion time series for the M2 and M4 tidal constituents. This analysis was carried out in a rolling series of 25-hour windows through the time series.

Water density was estimated as a function of temperature using the CTD data from all four cruises (Figure 3). Fitting a 2nd order polynomial to the data yielded a relationship between density and temperature (T (°C)) of:

$$\rho = 1026.84 + 0.10T - 0.01T^2 \tag{2}$$

with a root-mean-square deviation about the relationship of 0.03 kg m^{-3}. The relationship in (2) was used to convert temperatures on the interpolated grid of mean and instantaneous temperatures to densities, and to calculate values for the buoyancy frequency
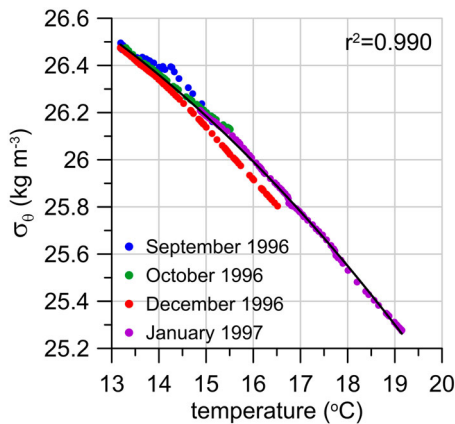
Figure 3. Density (σ_θ) versus temperature for all CTD data collected over the four cruises at station B1. The black solid line is the 2nd order polynomial fit to the data, with a root-mean-square deviation of the data around the fit of 0.03 kg m^{-3}.

and then time series of *PE* via (1). With a typical depth-mean value of N^2 of 5×10^{-5} s^{-2}, the rms error in the relationship in (2) results in an error in the depth integrated *PE* of about 15%. Values of *PE* in the upper 20 m and lower 10 m, i.e. above the uppermost RCM and below the deep RCM, were interpolated linearly to zero on the boundaries, as the vertical excursion of isotherms must approach zero at the boundaries.

Total internal wave energy is the sum of potential and kinetic energy contributions. Ideally a calculation of the wave kinetic energy (*KE*) would be made from a time series of current profiles (e.g. Sharples et al. 2001a). However, only having 2 RCMs on the mooring is not sufficient to allow calculation of the barotropic flow and the vertical structure of the baroclinic flow. Instead we can make use of a theoretical relationship (Fofonoff 1969) between internal tidal wave *PE* and *KE*, knowing the internal wave angular frequency (ω (s^{-1})) and the Coriolis frequency (f (s^{-1})):

$$\frac{PE}{KE} = \frac{(\omega^2 - f^2)}{(\omega^2 + f^2)} \tag{3}$$

The relationship in Equation (3) is applicable to a monochromatic, freely-propagating internal wave. Figure 2C demonstrates that most of the wave variability is in the M2 tidal constituent. Sharples et al. (2001a) calculated that the critical slope for the wave generation was 40 km offshore over the upper continental slope, and that the relation in (3) was consistent with an independent calculation of internal wave *KE* using current profile measurements. The total energy ($E = PE + KE$) for each of the tidal constituents of the internal tidal wave was calculated using the time series of *PE* and Equation (3) to calculate the corresponding time series of M2 and M4 *KE*. The total internal tide energy was then taken as the sum of the ($PE + KE$) for the M2 and M4 constituents.

We estimate the energy dissipation rate of the internal tide by assuming that all of the wave energy is dissipated between the mooring and the coast (a distance of 9.2 km), i.e. ignoring any reflection of energy back into the shelf (e.g. Largier 1994). Stevens et al. (2005)

found no evidence of internal wave reflection on the northeast New Zealand shelf. Previous observations of internal tidal wave propagation over the northeast shelf have yielded a wave speed of 0.3 m s^{-1} (Sharples et al. 2001a; Stevens et al. 2005), which when combined with the distance to the coast and the mean water density allows calculation of the mean wave energy dissipation rate, ε ($\text{m}^2 \text{ s}^{-3}$). The vertical eddy diffusivity, K_z ($\text{m}^2 \text{ s}^{-1}$), can then be estimated following the approach of Bouffard and Boegman (2013). A turbulence intensity parameter is calculated as

$$Re_b = \frac{\varepsilon}{\nu N^2} \tag{4}$$

with ν the molecular viscosity ($1.2 \times 10^{-6} \text{ m}^2 \text{ s}^{-1}$) and N^2 is the depth-mean of the squared buoyancy frequency from the mooring data. For $8.5 < Re_b < 400$ the vertical eddy diffusivity is calculated from (Osborn 1980):

$$K_z = \Gamma \frac{\varepsilon}{N^2} \tag{5}$$

with the flux dissipation coefficient (also called the mixing efficiency) Γ assigned a value 0.2. For $Re_b > 400$ the diffusivity is calculated from:

$$K_z = 4\nu Re_b^{0.5} \tag{6}$$

Nitrate data and nitrate fluxes

The consequences of internal wave-driven mixing for shelf biogeochemistry are estimated by considering the rate of upward diapycnal nitrate flux, F_{NO_3}:

$$F_{NO_3} = -K_z \frac{\Delta NO_3}{\Delta z} \tag{7}$$

where the vertical gradient in nitrate, ($\Delta NO_3/\Delta z$) (mmol m^{-4}), can be calculated using the nitrate data presented in Zeldis (2004). Using a similar method to that in Sharples et al. (2007) we use the nitrate and temperature data from the CTD profiles at station B1 to determine a linear relationship between nitrate concentration and temperature (Figure 4). The nitrate flux can then be calculated from:

$$F_{NO_3} = -K_z m \times \frac{\Delta T}{\Delta z} \tag{8}$$

where m (mmol $\text{m}^{-3} \,°\text{C}^{-1}$) is the gradient of the nitrate-temperature relationship in Figure 4 and the vertical temperature gradient is provided by the mooring data. For the temperature gradient we use the maximum value within a temperature profile, as this is usually where key nitrate gradients are at the base of the photic zone (e.g. Sharples et al. 2001b).

Results

The progression of the shelf temperature and salinity structure over the four cruises (Figure 5) shows a number of key, relevant features of the environment. Stratification
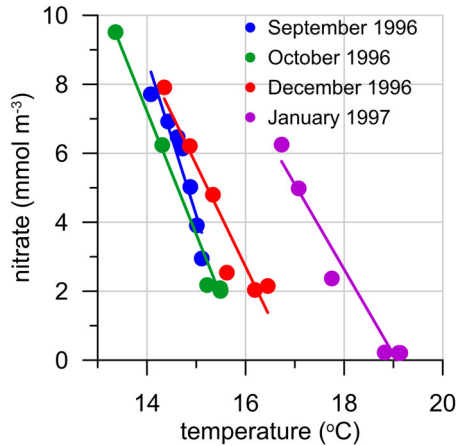
Figure 4. Nitrate versus temperature relationships for the CTD profiles at station B1 for each of the four cruises. Nitrate data from (Zeldis 2004).
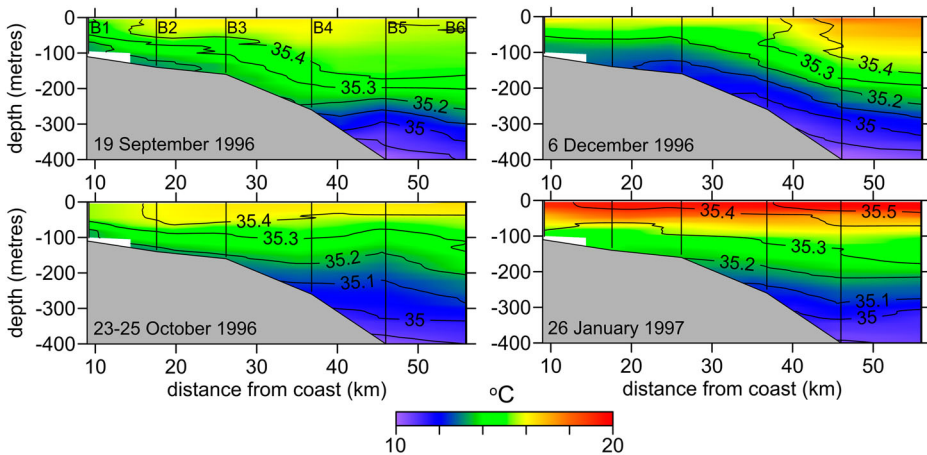

Figure 5. Cross-shelf sections of temperature (colours) and salinity (line contours, PSS78) for each of the four research cruises during the mooring deployment. For station positions, see Figure 1.

persisted throughout the mooring deployment, with strong vertical temperature gradients countering generally higher salinities at the surface compared to deeper in the water column. The along-slope flow of surface warm, salty subtropical water was particularly evident in December 1996, located over the slope at distance 50 km from the coast (Figure 5). Taking a salinity of 35.4 as indicating the transition from shelf water to subtropical water (Zeldis 2004), there is evidence in September 1996, October 1996 and most strongly in January 1997 of the subtropical water reaching onto the shelf. Thermal stratification was particularly strong in January 1997, with a shallow, warm surface layer with salinities close to 35.5 across most of the shelf. Upwelling of isotherms and isopycnals was seen in October 1996 and stronger upwelling was seen in December 1996, but upwelling was much weaker in January 1997.

Tidal variability in the temperature time series, as seen in Figure 2, could be caused by either (or both) of vertical oscillations of the temperature structure in response to an internal tidal wave or tidal excursion of a horizontal temperature gradient. A typical horizontal temperature gradient, based on the CTD data at stations B2 and B1 in October 1996 (Figure 5), was about 6×10^{-5} °C m^{-1}, while the surface RCM current data gives a mean tidal excursion in the cross-shelf direction of about 1.3 km. Thus, horizontal tidal flows could drive a semi-diurnal signal in temperature at the mooring of about 0.08°C. The mean temperature excursion seen at the mooring (Figure 3B) was about 0.32°C, showing that most of the signal is likely to have been caused by the internal tidal wave rather than horizontal excursion.

The mooring time series of raw temperature illustrates the progression to increasing thermal stratification from September 1996 to January 1997, with very warm surface water arriving around 27th December (Figure 6). This warm water marks the annual event of wind-driven transfer of surface subtropical water from over the slope onto the shelf (e.g. Sharples 1997), driven by a strong north-westward component to the wind stress between 26th and 30th December. Superimposed on the long-term temperature changes in Figure 6 can be seen the persistent fine structure of the semi-diurnal tidal oscillations associated with the passage of the internal tidal wave.

Analysis of this temperature structure using the harmonic fitting procedure described earlier produced a time series of the vertical pattern of tidal excursion amplitudes for the isotherms for the M2 and M4 tidal constituents (Figure 7). The time series is dominated by the M2 tidal constituent, with peak excursion amplitudes reaching 20–25 m, and so a peak-trough range of isotherm movement of 40–50 m. By contrast the M4 excursion amplitude reaches 10–12 m. Maximum excursion amplitudes tend to be close to the middle of the water column, consistent with the mode 1 structure of the main internal tidal wave (e.g. Sharples et al. 2001a). The strength of the internal tidal waves is clearly highly variable, with two notable periods of consistently low wave amplitudes in late October/early November and in early January.

The relative contributions of the M2 and M4 tidal constituents to the depth-integrated *PE*, and the highly variable nature of the internal tide *PE*, are shown in Figure 8A,B. Peaks in the M2 *PE* typically reach 150 J m^{-2}, and as high as 300 J m^{-2}, which is similar to that
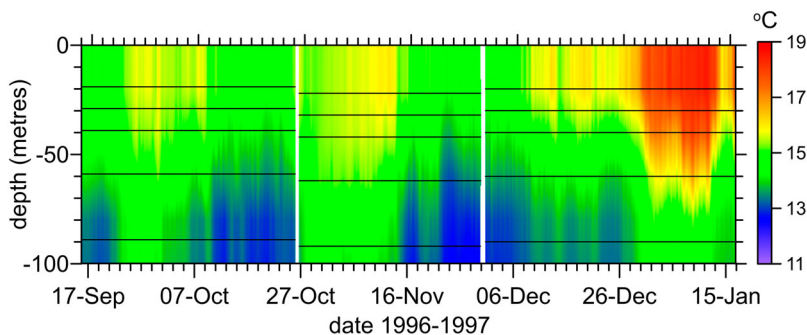

Figure 6. Time series of the vertical structure of temperature at the mooring. Horizontal lines mark the depths of the temperature loggers and RCMs. The white gaps on 26th October and 30th November are data gaps during mooring servicing.
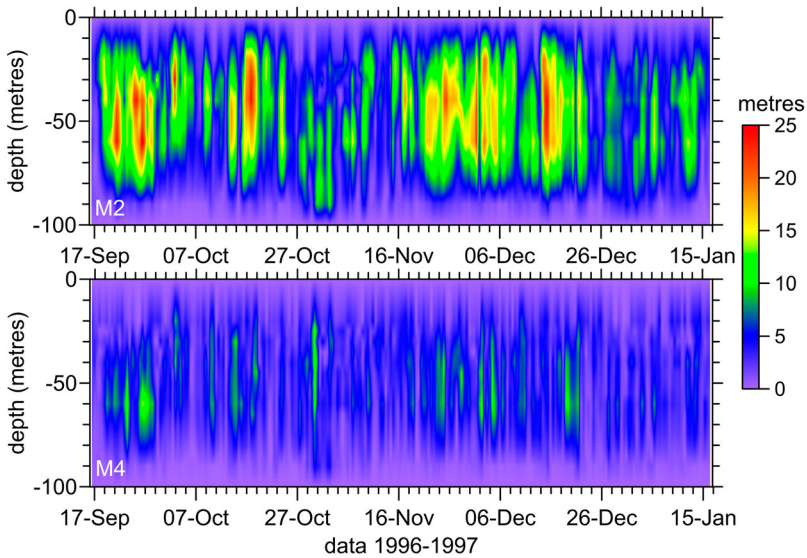
Figure 7. Amplitude of the vertical excursion of isotherms based on harmonic analysis for the M2 (upper panel) and M4 (lower panel) tidal constituents.

seen in the on-shelf mooring in Sharples et al. (2001a). Combining the potential energy data with calculation of the kinetic energies for the two tidal constituents (using Equation(3)) yields the total energy in the internal tidal wave (Figure 8C). Not surprisingly variability in the total energy is dominated by the potential energy in the M2 constituent, with mean energy of about 190 ± 145 (1 s.d.) J m^{-2}, and peak energies reaching 600–800 J m^{-2}. There was a particularly marked reduction in the water column PE and total energy from about 27th October 1996 to 15th November 1996.

The mean rate of energy dissipation (Figure 9A) was 0.007 (± 0.005, 1 s.d.) W m^{-2}, which is consistent with previous values from much shorter time series on the northeast shelf of New Zealand (0.015 ± 0.010 W m^{-2} (Sharples et al. 2001a) and 0.007 W m^{-2} (Stevens et al. 2005)). Calculation of the turbulence intensity parameter (Equation (4)) indicates that the system was almost always in the energetic regime with $Re_b > 400$ (Figure 9B); calculation of the vertical eddy diffusivity (Figure 9C) shows that using the Osborn relation (Equation (5)) would result in an overestimate of scalar mixing. The mean diffusivity over the entire deployment based on the Osborn relation is 3.2×10^{-4} ($\pm 2.4 \times 10^{-4}$, 1 s.d.) m^2 s^{-1}, while application of Equations (5) and (6) depending on the value of Re_b yields a mean diffusivity of 1.6×10^{-4} ($\pm 0.7 \times 10^{-4}$, 1 s.d.) m^2 s^{-1}. For most of the deployment the turbulent intensity results in the use of Equation (6) for calculation of the diffusivity, which both lowers the typical diffusivity and reduces the range of the variability in diffusivity. Using Equation (8), with the values for m taken from the regressions in Figure 4, the vertical nitrate flux can be estimated associated with each of the research cruises. Taking the mean diffusivities and vertical temperature gradients over 7 days about each cruise (or the last 7 days of the mooring deployment for the January cruise) yields nitrate fluxes of 1.7 ± 0.8, 1.6 ± 0.8, 2.0 ± 0.3 and 2.2 ± 0.9 mmol m^{-2} day^{-1} for the cruises in September, October, December and January respectively. These fluxes are less than the flux reported by Sharples et al. 2001a, who calculated a flux of 12 mmol m^{-2}
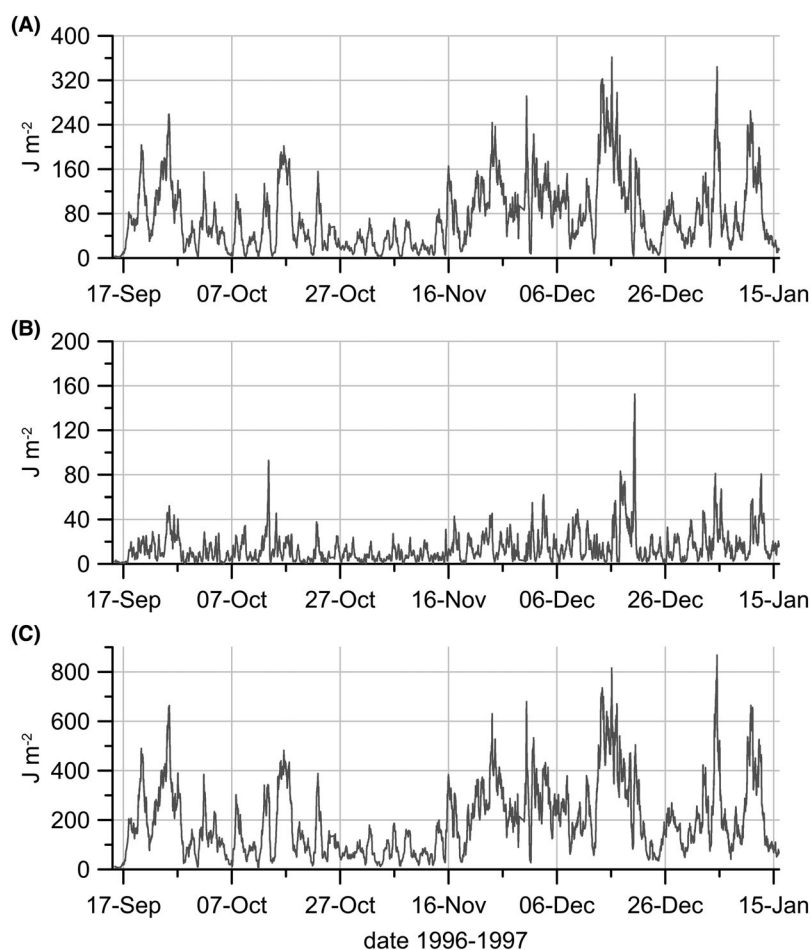
Figure 8. A, Depth-integrated potential energy in the internal tidal wave (*PE* in Equation (1)) for the M2 tidal constituent. **B,** Depth-integrated potential energy for the M4 tidal constituent. **C,** Depth-integrated total energy in the internal tidal wave, using the time series in A and B with Equation (3).

day^{-1} over a short mooring deployment in summer. Much of the discrepancy is a result of a higher estimate of the diffusivity by Sharples et al. (2001a), based on microstructure measurements over a single tidal cycle. Over this much longer mooring deployment the perhaps surprising result is that the flux did not change markedly, and indeed appears to have been strongest during the time of strongest stratification; the reasons for this will be discussed below.

Discussion

A 4-month time series of thermal structure on the shelf of northeast New Zealand has illustrated marked variability in the vertical oscillations of the isotherms and in the wave potential energy. While the wave is known to steepen and break (Sharples et al. 2001a) the M2 tidal constituent dominates over the M4 harmonic; overall the mean *PE* at the M2 frequency was 74.5 J m^{-2}, compared to an M4 contribution of 14.5 J m^{-2}.
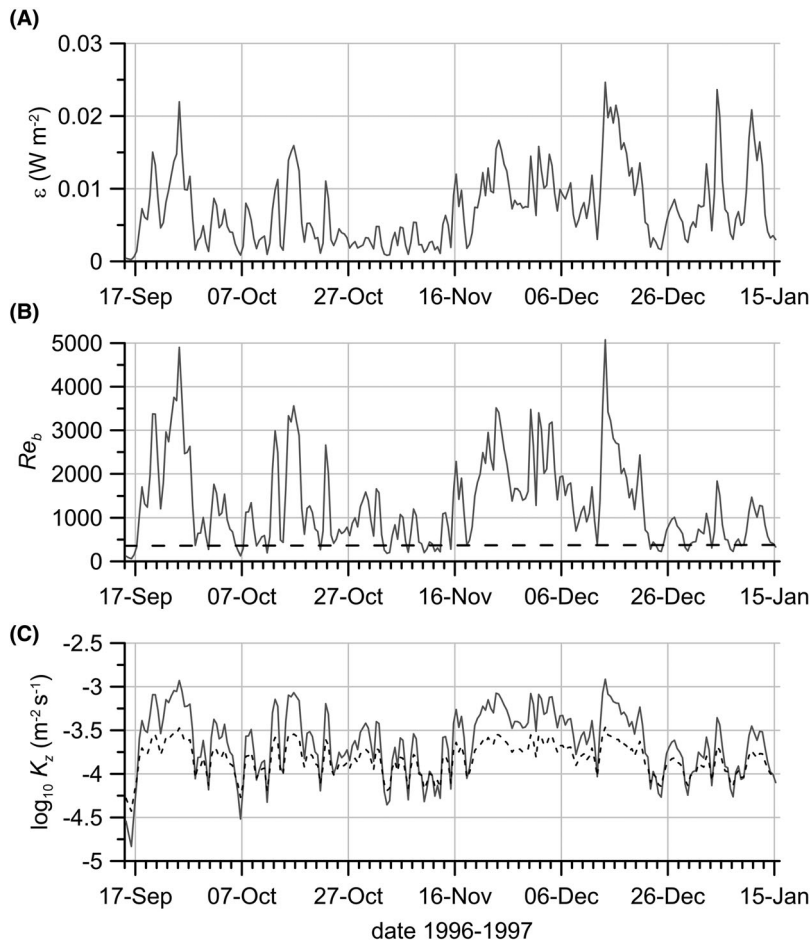
Figure 9. A, Time series of internal tidal wave dissipation, assuming that all wave energy is dissipated between the mooring and the coast. **B,** Turbulence intensity parameter (Equation (4)). **C,** Time series of depth-mean vertical eddy diffusivity, K_z (from Equations (5) (solid line) and (6) (dashed line)). The horizontal dashed line in B marks $Re_b = 400$.

The following discussion will focus on first on determining if there are any consistent or significant links between internal wave energy and the physical structure and forcing of the shelf. We will then consider the implications of the wave energy for vertical mixing and diapycnal nutrient fluxes on the shelf.

The resulting time series of total wave energy can be compared to time series of wind forcing, local stratification, and the stage of the spring-neap tidal cycle (Figure 10). A sustained period of moderate wind stress between 23rd and 29th October 1996 (Figure 10A) resulted in a marked reduction in stratification (Figure 10B) and a reduction in the upwelling slope of the isotherms. The CTD profile at station B1 conducted on 25th October showed a vertically-mixed surface layer to a depth of 50 m, and a temperature difference between depths of 20 and 90 m of 2.2°C. The mooring data (Figure 10B) suggest that the stratification was further eroded, reaching only 0.5°C by 29th October. This reduction in stratification reduced the energy in the internal tidal wave (Figure 10D), with the internal
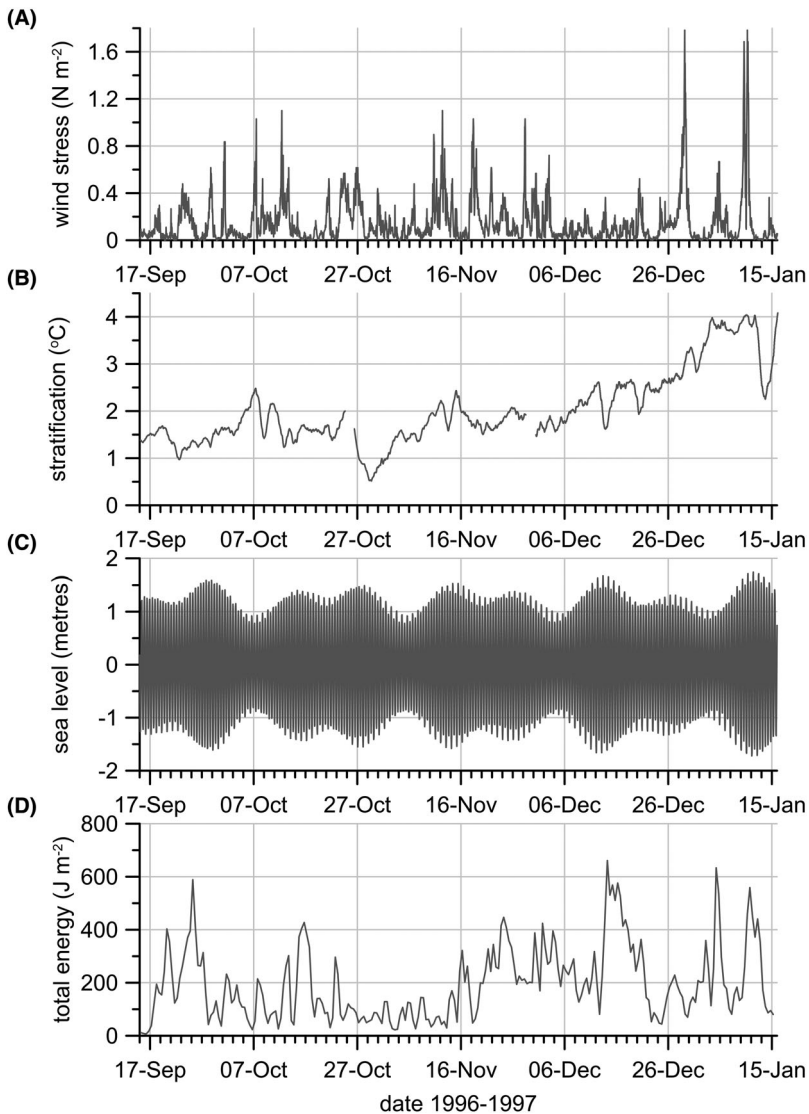
Figure 10. A, Time series of surface wind stress, calculated from the wind data available from the Mokohinau Islands. **B,** Time series of local stratification, calculated as the difference between low frequency near-surface and near-bed temperatures measured by the RCMs on the mooring. **C,** Tidal variability in sea level for Auckland harbour. **D,** Time series of the total internal tidal wave energy ($PE + KE$) for both M2 and M4 tidal constituents. Sea level in C was calculated for Auckland harbour (see Figure 1) using https://tides.niwa.co.nz/.

wave energy recovering from about 14th November. Such a wind-driven mixing event and its effect on the internal tide is similar to that described in Sharples et al. (2001a), though with a significantly lengthened recovery time in the internal wave compared to the return of the stratification. A similar response to a wind event can also be seen at the end of the time series, with a sharp, strong wind event on 11th January markedly reducing the stratification and the internal wave energy.

An analysis of the correlation between the magnitude of the wind stress and wave energy yields $r = -0.05$ with zero time lag and switching to $r = 0.08$ with a lag of 3 days. A correlation with the along-shelf component of the wind stress yields $r = -0.08$ with little change with time lag. Correlation between stratification (maximum buoyancy frequency) and wave energy show $r = 0.20$ to 0.22 as the time lag changes from 0 days to 2 days. Thus, there is negligible consistent link through the time series between wave energy and wind-driven mixing or along-shelf wind stress. There is some correlation with stratification: weaker stratification is associated with lower internal wave energy, which is consistent with the role of stratification in propagating internal waves.

In Figure 10C,D there does appear to be some link between some spring tides and peaks in the internal wave energy, which would be expected as the barotropic tide is the fundamental driver of the internal tide. The daily maximum tidal current speed was calculated by performing a harmonic analysis of the entire time series of the along-shelf current data from the surface RCM for the M2, S2 and N2 tidal constituents (i.e. the spring-neap cycle, modulated by the N2 lunar elliptic constituent). Correlation of the internal wave energy with the predicted daily maximum tidal current speed was very weak, with a maximum $r = 0.17$ at zero time lag.

Overall, therefore, while it might appear that there are some small correlations between wave energy and the physical environment, all of the correlations are weak and there is little clear predictability in the time series of internal tide energy. This result is consistent with other long time series of internal wave behaviour (e.g. Cottier et al. 2004), and the general finding that internal tides are usually unpredictable (Nash et al. 2012). The likely generation site for the internal tidal wave is about 40 km offshore over the continental slope, in a depth of 600–700 m (Sharples et al. 2001a). Internal tidal wave energy will be set at the generation site and will not correlate strongly with conditions local to the mooring. Energy at the mooring will depend on the fraction of initial internal wave energy propagating onto the shelf, reflection of wave energy at the upper slope, and dissipation of wave energy as it moves through the varying water column density structure across the shelf edge and shelf. The only robust observation from the northeast shelf mooring results is that internal tide energy was reduced markedly following a strong, downwelling-favourable wind mixing event (i.e. late October 1996).

Periods of generally low diffusivities are associated both with the low wave energy following wind-mixing in late October, and also with the stronger stratification associated with the on-shelf transport of the warm surface subtropical water in early January (Figure 9B,D). However, low diffusivity does not necessarily translate into low diapycnal nitrate flux. Table 1 summarises the values of parameters that combine to provide the

Table 1. Data used in the calculation of vertical nitrate fluxes driven by the internal tide.

Cruise month	$\frac{\Delta NO_3}{\Delta z}$ (mmol m^{-4})	$\frac{\Delta T}{\Delta z}$(°C m^{-1})	N^2 (s^{-2})	E (J m^{-2})	Kz (m^2 s^{-1})	FNO_3 (mmol m^{-2} day^{-1})
September	−0.117	0.026	3.3×10^{-5}	172	1.7×10^{-4}	1.7
October	−0.119	0.033	3.5×10^{-5}	105	1.4×10^{-4}	1.6
December	−0.111	0.037	4.4×10^{-5}	243	2.0×10^{-4}	2.0
January	−0.193	0.077	9.4×10^{-5}	265	1.3×10^{-4}	2.2

Notes: Values for ($\Delta NO_3/\Delta z$) come from the regressions in Figure 4 combined with ($\Delta T/\Delta z$). All parameters are mean values over 7 days centred on the cruise CTD survey of line B, except for January 1997 when the last 7 days of the mooring deployment are used.

nitrate flux for ±3 days around the times of each of the CTD surveys along line B. Note that the January cruise and mooring recovery took place at the end of the month, while the useful mooring data finished in mid-January; we have used early January for the nitrate flux calculation as relevant for the situation when the subtropical water has capped the shelf.

The lowest fluxes observed were in September and October 1996, associated with low internal tidal energy and low vertical temperature gradient; internal tidal energy was lowest in October as a result of the strong winds. However, fluxes prior to the January 1997 subtropical intrusion probably do not indicate a limiting factor to the primary production, as nitrate concentrations were still close to 2 mmol m^{-3} at the sea surface, i.e. phytoplankton would not have been nitrate-limited (Eppley et al. 1969) and the nitrate flux was able to overcome the uptake requirements throughout the water column. Instead the importance of the internal tide mixing in spring and early summer probably lies with the role that it plays in controlling the light environment experienced by the phytoplankton. The nitrate flux in January 1997 is more biogeochemically important, as the intrusion of the oligotrophic subtropical water led to a surface later deplete in nitrate (e.g. the warm water nitrate concentrations in January 1996; Figure 4); in that case the nitrate flux will be a limiting factor to new primary production in the photic zone. The stronger stratification in January ($N^2 = 9.4 \times 10^{-5}$ s^{-2} compared to $\leq 4.4 \times 10^{-5}$ s^{-2} in September to December) was associated with a reduction in K_z, but the effect on the nitrate flux was more than compensated for by the associated stronger nitrate gradient (Table 1). The internal wave energy was also stronger in January (Table 1). The stratification at depth over the upper slope was not affected by the subtropical intrusion in January, with deep water values of N^2 virtually unchanged across all four CTD surveys, so conversion of barotropic tidal energy into the internal tidal wave would have been similar. The stronger wave energy on the shelf in January was perhaps instead related to the stronger upper ocean stratification aiding the propagation of internal wave energy. It is generally expected that as the climate warms, near-surface stratification will strengthen and result in a reduction in the nutrient supply to the surface ocean (Sarmiento et al. 2004; Steinacher et al. 2010). This simple link between warming and nutrient supply has been questioned. Climate warming could also alter wind and buoyancy forcing as well as the advective supply of nutrients (Lozier et al. 2011). The results here suggest that strengthening stratification could also lead to more energy in the internal tide over the shelf and also steeper nutrient gradients, both of which could counter a reduction in nutrient supply to the surface ocean.

Disclosure statement

No potential conflict of interest was reported by the authors.

ORCID

Jonathan Sharples 🄳 http://orcid.org/0000-0002-7031-3593

References

Bouffard D, Boegman L. 2013. A diapycnal diffusivity model for stratified environmental flows. Dynamics of Atmospheres and Oceans. 61–62:14–34.

Chiswell SM, Moore MI. 1999. Internal tides near the Kermadec ridge. Journal of Physical Oceanography. 29(5):1019–1035.

Cottier F, Inall M, Griffiths C. 2004. Seasonal variations in internal wave energy in a Scottish sea loch. Ocean Dynamics. 54(3–4):340–347.

Dewey R, Richmond D, Garrett C. 2005. Stratified tidal flow over a bump. Journal of Physical Oceanography. 35(10):1911–1927.

Embling CB, Sharples J, Armstrong E, Palmer MR, Scott BE. 2013. Fish behaviour in response to tidal variability and internal waves over a shelf sea bank. Progress in Oceanography. 117:106–117.

Eppley RW, Rogers JN, McCarthy JJ. 1969. Half-saturation constants for uptake of nitrate and ammonium by marine phytoplankton. Limnology and Oceanography. 14(6):912.

Fofonoff NP. 1969. Spectral characteristics of internal waves in the ocean. Woods Hole (MA): Woods Hole Oceanographic Institution. 19 p.

Garrett C, Kunze E. 2007. Internal tide generation in the deep ocean. Annual Review of Fluid Mechanics. 39:57–87.

Largier JL. 1994. The internal tide over the shelf inshore of Cape Point Valley, South-Africa. Journal of Geophysical Research-Oceans. 99(C5):10023–10034.

Ledwell JR, Montgomery ET, Polzin KL, St Laurent LC, Schmitt RW, Toole JM. 2000. Evidence for enhanced mixing over rough topography in the abyssal ocean. Nature. 403(6766):179–182.

Lozier MS, Dave AC, Palter JB, Gerber LM, Barber RT. 2011. On the relationship between stratification and primary productivity in the North Atlantic. Geophysical Research Letters. 38:L18609. doi:10.1029/2011GL049414

Munk W, Wunsch C. 1998. Abyssal recipes II: energetics of tidal and wind mixing. Deep-Sea Research Part I-Oceanographic Research Papers. 45(12):1977–2010.

Nash JD, Shroyer EL, Kelly SM, Inall ME, Duda TF, Levine MD, Jones NL, Musgrave RC. 2012. Are any coastal internal tides predictable? Oceanography. 25(2):80–95.

New AL, Pingree RD. 1990. Evidence for internal tidal mixing near the shelf break in the Bay of Biscay. Deep-Sea Research Part a-Oceanographic Research Papers. 37(12):1783–1803.

Noble M, Mullineaux LS. 1989. Internal tidal currents over the summit of cross seamount. Deep-Sea Research Part a-Oceanographic Research Papers. 36(12):1791–1802.

Osborn TR. 1980. Estimates of the local-rate of vertical diffusion from dissipation measurements. Journal of Physical Oceanography. 10(1):83–89.

Palmer MR, Inall ME, Sharples J. 2013. The physical oceanography of Jones Bank: a mixing hotspot in the Celtic Sea. Progress in Oceanography. 117:9–24.

Rudnick DL, Boyd TJ, Brainard RE, Carter GS, Egbert GD, Gregg MC, Holloway PE, Klymak JM, Kunze E, Lee CM, et al. 2003. From tides to mixing along the Hawaiian ridge. Science. 301 (5631):355–357.

Sarmiento JL, Slater R, Barber R, Bopp L, Doney SC, Hirst AC, Kleypas J, Matear R, Mikolajewicz U, Monfray P, et al. 2004. Response of ocean ecosystems to climate warming. Global Biogeochemical Cycles. 18(3):GB3003.

Sharples J. 1997. Cross-shelf intrusion of subtropical water into the coastal zone of northeast New Zealand. Continental Shelf Research. 17(7):835–857.

Sharples J, Grieg MJN. 1998. Tidal currents, mean flows, and upwelling on the north-east shelf of New Zealand. New Zealand Journal of Marine and Freshwater Research. 32:215–231.

Sharples J, Moore CM, Abraham ER. 2001a. Internal tide dissipation, mixing, and vertical nitrate flux at the shelf edge of NE New Zealand. Journal of Geophysical Research-Oceans. 106 (C7):14069–14081.

Sharples J, Moore CM, Hickman AE, Holligan PM, Tweddle JF, Palmer MR, Simpson JH. 2009. Internal tidal mixing as a control on continental margin ecosystems. Geophysical Research Letters. 36:L23603.

Sharples J, Moore CM, Rippeth TP, Holligan PM, Hydes DJ, Fisher NR, Simpson JH. 2001b. Phytoplankton distribution and survival in the thermocline. Limnology and Oceanography. 46 (3):486–496.

Sharples J, Tweddle JF, Green JAM, Palmer MR, Kim YN, Hickman AE, Holligan PM, Moore CM, Rippeth TP, Simpson JH, et al. 2007. Spring-neap modulation of internal tide mixing and vertical nitrate fluxes at a shelf edge in summer. Limnology and Oceanography. 52(5):1735–1747.

Sherwin TJ. 1988. Analysis of an internal tide observed on the Malin shelf, north of Ireland. Journal of Physical Oceanography. 18(7):1035–1050.

Stanton BR. 1977. Preliminary-observations of internal tide over shelf west of New-Zealand. New Zealand Journal of Marine and Freshwater Research. 11(4):703–712.

Steinacher M, Joos F, Frolicher TL, Bopp L, Cadule P, Cocco V, Doney SC, Gehlen M, Lindsay K, Moore JK, et al. 2010. Projected 21st century decrease in marine productivity: a multi-model analysis. Biogeosciences. 7(3):979–1005.

Stevens CL, Abraham ER, Moore CM, Boyd PW, Sharples J. 2005. Observations of small-scale processes associated with the internal tide encountering an island. Journal of Physical Oceanography. 35(9):1553–1567.

Stevens CL, Sutton PJH, Law CS. 2012. Internal waves downstream of Norfolk Ridge, Western Pacific, and their biophysical implications. Limnology and Oceanography. 57(4):897–911.

Tuerena RE, Williams RG, Mahaffey C, Vic C, Green JAM, Garabato ACN, Forryan A, Sharples J. 2019. Internal tides drive pulses of nutrients into the deep chlorophyll maximum over mid-ocean ridges. Global Biogeochemical Cycles 33(8):995–1009. doi:10.1029/2019GB006214

Tweddle JF, Sharples J, Palmer MR, Davidson K, McNeill S. 2013. Enhanced nutrient fluxes at the shelf sea seasonal thermocline caused by stratified flow over a bank. Progress in Oceanography. 117:37–47.

Vennell R, Moore M. 1993. Acoustic doppler current profiler measurements of the semi-diurnal internal tide on the west-coast of New-Zealand. New Zealand Journal of Marine and Freshwater Research. 27(1):31–38.

Vic C, Garabato ACN, Green JAM, Spingys C, Forryan A, Zhao ZX, Sharples J. 2018. The lifecycle of semidiurnal internal tides over the Northern Mid-Atlantic ridge. Journal of Physical Oceanography. 48(1):61–80.

Waterhouse AF, Kelly SM, Zhao ZX, MacKinnon JA, Nash JD, Simmons H, Brahznikov D, Rainville L, Alford M, Pinkel R. 2018. Observations of the Tasman Sea internal tide beam. Journal of Physical Oceanography. 48(6):1283–1297.

Waterhouse AF, MacKinnon JA, Nash JD, Alford MH, Kunze E, Simmons HL, Polzin KL, St Laurent LC, Sun OM, Pinkel R, et al. 2014. Global patterns of diapycnal mixing from measurements of the turbulent dissipation rate. Journal of Physical Oceanography. 44(7):1854–1872.

Witman JD, Leichter JJ, Genovese SJ, Brooks DA. 1993. Pulsed phytoplankton supply to the rocky subtidal zone - influence of internal waves. Proceedings of the National Academy of Sciences of the United States of America. 90(5):1686–1690.

Wunsch C, Hendry R. 1972. Array measurements of the bottom boundary layer and the internal wave field on the continental slope. Geophysical Fluid Dynamics. 4(1):101–145.

Zeldis JR. 2004. New and remineralised nutrient supply and ecosystem metabolism on the north-eastern New Zealand continental shelf. Continental Shelf Research. 24(4–5):563–581.

Zeldis JR, Walters RA, Greig MJN, Image K. 2004. Circulation over the northeastern New Zealand continental slope, shelf and adjacent Hauraki Gulf, during spring and summer. Continental Shelf Research. 24(4–5):543–561.